J. Fluid Mech. (1975), *vol.* 72, *part* 3, *pp.* 513–527
Printed in Great Britain

The experimental wave resistance of an accelerating two-dimensional pressure distribution

By LAWRENCE J. DOCTORS
School of Mechanical and Industrial Engineering,
University of New South Wales, Kensington

(Received 10 March 1975)

A series of experiments designed to measure the wave resistance of an accelerating two-dimensional air-cushion vehicle is described. A model was towed at a constant acceleration from rest over water of various depths. In addition, the effects of different levels of acceleration and different cushion pressures were examined. The results are compared with linearized potential-flow theory and show particularly encouraging agreement. The predicted humps and hollows in the curve of wave resistance *vs.* time are verified, but with a small shift with respect to time. Also, the theoretical region of negative wave resistance in water of finite depth is demonstrated.

1. Introduction

One of the problems in the design of an air-cushion vehicle (ACV) is the requirements to overcome the drag at the hump speed. The drag is generally considered to consist of the following components: the aerodynamic profile drag on the craft, which is approximately proportional to the square of the speed, the momentum drag due to the ingestion of cushion air from the surrounding atmosphere into the moving vehicle, which is proportional to the craft speed, the wave drag, and the other interactive effects, including water contact and spray.

The wave-drag component is found to exhibit a main peak (or hump) at a Froude number which depends on the water depth and craft planform shape. In some cases, those of relatively high cushion pressure, it is this hump which imposes the minimum requirement on the engine power, since the wave drag (and thus the total drag) drops beyond this speed before finally rising again.

The wave resistance of an air-cushion vehicle can be studied by assuming its action to be hydrodynamically equivalent to that of a pressure distribution acting on the free surface of the water. Naturally, this idealization neglects physical contact between the skirt of the craft and the water, and it does not allow the existence of any spray.

For example, Havelock (1932) derived the wave-resistance expression for a general pressure distribution travelling at a constant speed. This theoretical work was later extended by Lunde (1951) to include the effect of water of finite

depth. Barratt (1965) presented numerical results for a pressure distribution of constant intensity acting on a rectangular or elliptical area. The most striking feature of his results is the series of humps and hollows in the wave-resistance curve, the main hump occurring in deep water at a Froude number of approximately 0·56. The humps are shifted to a lower Froude number in water of restricted depth. In sufficiently shallow water, the main hump occurs at a depth Froude number of unity.

The work of Newman & Poole (1962) included the effect of transversely restricted water. Oscillations in the wave-resistance curve were displayed as well as the interference due to the sides of the channel.

The humps and hollows are physically due to the production of waves, principally by the forward and aft ends of the pressure distribution. These waves have a large component transverse to the direction of motion and may therefore combine or cancel each other at the stern. This depends on the speed of advance of the ACV. When the waves combine, the elevation of the water near the stern is low, so that the craft trims positively, and the wave resistance makes its presence felt on the craft through this mechanism.

The above-mentioned publications all represent an application of potential-flow theory with linearized free-surface conditions. The theory predicts an infinite number of oscillations from the main hump down to zero speed.

To examine this phenomenon, experiments on models have been made by Everest (1966*a*, *b*) and Hogben (1966). One of the main difficulties indicated was the separation of the wave-drag component from the measured total drag. The aerodynamic drag on the model and the momentum drag were estimated and subtracted from the total. The remainder was considered to be the wave drag and compared with the theory. No account of water contact was attempted, although Everest (1966*a*) experimented with a thin polythene sheet floating on the water, designed to eliminate spray. No doubt tension within this sheet would be a source of error.

The general agreement appeared to be quite good with regard to the overall range of values of the wave resistance. Large scatter in the data was evident, being due to the spray and water contact. The main hump and the secondary one were displayed, and were out of phase with the theoretical values by up to 0·05 on the Froude-number scale. The absence of the other humps was attributed to nonlinearity by Hogben (1965).

Further experiments were performed by Everest & Willis (1958) and Everest & Hogben (1966, 1967, 1969). Here the wave resistance was measured directly by an analysis of the wave pattern. Such techniques, using wave-elevation probes, were described by Eggers, Sharma & Ward (1967). This method produced far less scatter in the data.

Turning now to the problem of unsteady motion, some experiments were carried out on models in water of finite depth by Everest & Hogben (1967). Acceleration levels of 0·0014 g and 0·0022 g were maintained in water of depth 0·215 of the craft length. In the former case the hump drag was reduced (the reduction in wave drag was in fact greater because the inertia of the model must also be considered). In the second case the measured drag was greater owing to

substantial water contact. The practical implication of this is that the critical hump-drag condition might be alleviated by a suitable choice of acceleration.

The wave resistance of an ACV starting from rest has been computed from the theoretical point of view by Doctors & Sharma (1972). Acceleration had the effect of reducing the higher-order oscillations and shifting them to a larger Froude number. It was also shown that, by using a pressure distribution with smoothing at the forward and aft edges, the low-speed oscillations could be eliminated. However, somewhat unrealistically large amounts of smoothing were required to eliminate all but the main two humps in order to tally with steady-state experiments. Thus nonlinearity and viscosity were confirmed as being important features at low speed. Another result predicted was that a two-dimensional pressure band experiences negative resistance during part of the accelerated motion.

The theory was extended by Doctors (1972) to include the effect of side as well as end tank walls for unsteady motion in a restricted area. The effects of wall reflexions were depicted there. Some applications of the unsteady wave-resistance calculations were given by Doctors & Sharma (1973) and illustrated by an ACV accelerating up to its cruising speed.

The aim of the present work is to test the theory for unsteady motion, since experimental work on ACV's to date has been restricted to steady motion. It is felt that agreement between theory and experiment should be better in the unsteady case, since strong interference effects and large wave slopes will not have time to be generated.

2. Experimental equipment

The general arrangement of the equipment is shown in figure 1. The tank was 20 ft long and 2 ft wide and could be filled to a depth of 1 ft. The construction consisted basically of a steel-angle framework. The frames were fitted with wooden spacing strips onto which the plywood lining was attached. This method allowed accurate fixing of the internal tank dimensions as well as its levelling.

Although the carriage rails were laid (also on spacers) to within a height accuracy of 0·02 in., to allow smooth motion of the carriage, the two wheels on one side were mounted on a separate section which pivoted about its centre on the rest of the carriage frame. Thus all four wheels continuously remained in contact with the track throughout the motion.

The drive system was designed around a falling-weight concept. Hence the basic type of acceleration pattern, namely a constant one, could easily be studied. A series of equally spaced electrical contacts along one side of the channel and a wiper on the carriage were connected to an event marker on an ultra-violet recorder. In this way, the constancy of the acceleration was verified. The acceleration throughout a run had a maximum deviation of 0·5% from the mean value for that run. This indicated the minor influence of hydrodynamic and aerodynamic drag on the motion of the model, as well as frictional variations in the cables, etc. (The inertia of the moving parts of the system was designed to be relatively high in order to produce this result.) It was also found that the

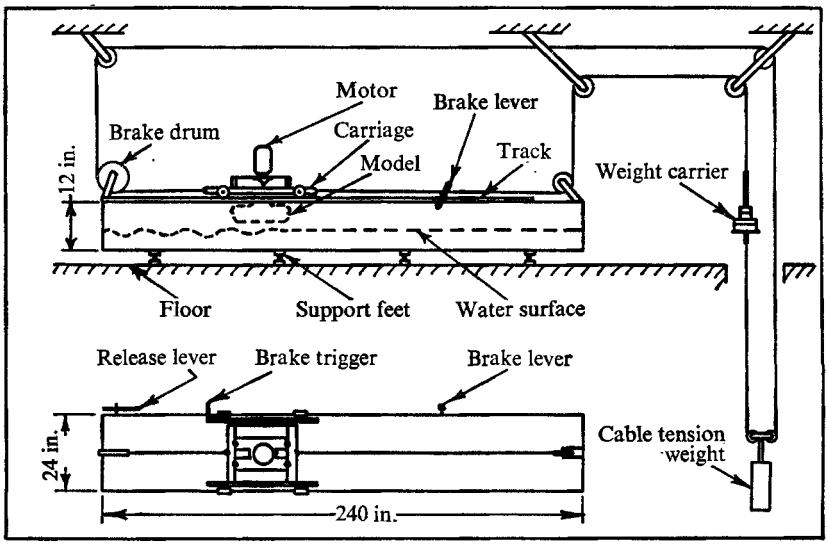

FIGURE 1. Schematic layout of tank, carriage and cable system.

weights could be selected to give a required acceleration level usually to within 1 % but occasionally with a 2 % error.

The continuous cable, passing around a total of eight pulleys, was tensioned by a weight, as shown in figure 1. One of the pulleys was combined with a brake drum. A pair of diametrically opposed brake shoes were pulled together by a tension spring, but kept off the drum surface by a caliper. The carriage, on reaching the end of its run, would throw the brake lever mounted at the side of the tank, which released the caliper, allowing the shoes to bear against the drum and thus bring the carriage to a halt. A release lever designed to impart a clean start to the carriage motion was also fitted.

The ACV model is shown in figure 2. For the sake of simplicity, and because of the resulting reduction in the data analysis, a two-dimensional model spanning the channel was built as a first stage of the project. On the other hand, the tank had to be sufficiently wide to minimize side-wall interference (see Doctors 1972) for a three-dimensional model, yet to be built. A third advantage was that the basic phenomena of ACV wave interference are more strongly displayed in two dimensions.

The radial-flow fan was driven by a 0·5 h.p. shunt-wound d.c. electric motor with a nominal speed of 2850 r.p.m. when supplied with 240 V. The model was fitted with an entry bell mouth and a set of vanes to ensure a uniform distribution of air to the fore and aft nozzles. Finally, in order to facilitate the adjustment of the height of the model above the water surface, a set of four replaceable spacers was used to attach it to the carriage frame.

It was decided to measure the wave resistance directly, by analysis of the free-surface elevation. As mentioned previously, this method minimized the degree of scatter in the experimental results for steady motion. Thus the idea of measuring the variation in the towing-cable tension was considered impractical

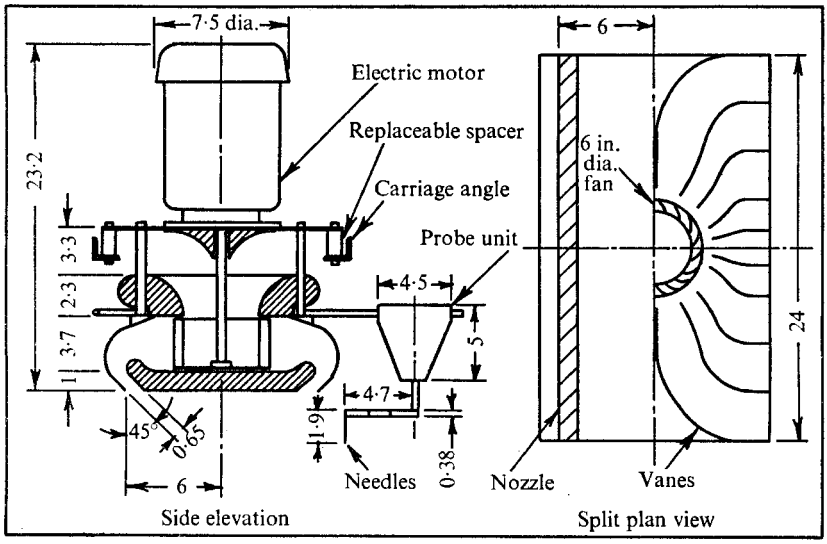

FIGURE 2. General arrangement of ACV model. Dimensions in inches.

owing to the difficulty of accurately estimating the other drag components to be subtracted from it. The probe itself consisted of a pair of stainless-steel needles 0·034 in. in diameter and separated by 0·40 in. These were electrically insulated from each other and were attached to an extension arm to allow probing under the model. The determination of the wave elevation was based on the variation of the electrical conductance between the probe needles with the depth of immersion. Calibration was achieved by raising and lowering the needles via a screw-drive system within the probe unit. The wave elevation at different longitudinal positions relative to the model was obtained by shifting the probe unit on a pair of shafts.

The needles were connected electrically such that the resistance of the water between them was in parallel with one of the four arms of a Wheatstone bridge. Each arm had a resistance of 560 Ω, and the bridge was supplied by a 3000 Hz signal of 5 V. The resulting bridge imbalance, due to variations in wave height, was amplified and rectified. The signal was then used to drive an ultra-violet galvanometer with a natural frequency of 450 Hz, this being considerably higher than the component frequencies of the wave system.

3. Experimental analysis

The wave resistance may be defined directly as the longitudinal component of the cushion pressure force acting on the water surface. This might be more accurately referred to as the pressure resistance and for an inviscid fluid is equal to the rate at which the mechanical energy in the waves is increased divided by the craft speed, if the ACV is travelling at a constant speed. In a real situation there is, of course, some dissipation of that energy into heat. For an unsteady situation, an additional component of work due to the pressure acting against

the vertical motion of the surface exists. This second term was computed by Doctors & Sharma (1972). The resistance per unit width of the two-dimensional model is therefore

$$R = \int p(x) \frac{\partial \zeta}{\partial x} dx, \tag{1}$$

where the cushion pressure p varies with the longitudinal distance x, measured forward of the model centre. The wave elevation above the undisturbed level is ζ.

Wave profiles were taken at different values of x symmetrically placed fore and aft of the model centre. It is only necessary to take profiles in the region where p varies, namely, near the ends.

This point may be demonstrated by carrying out a partial integration of (1), which yields

$$R = [p(x)\,\zeta(x)]_{-\infty}^{\infty} - \int_{-\infty}^{\infty} \zeta \frac{\partial p}{\partial x} dx.$$

The first term is zero. It is seen that, in the central region where p is constant, there is no contribution to the integral, and no profiles need to be taken there. The problem of numerical differentiation of ζ is also avoided, since p is a relatively smooth function of x. This equation was numerically approximated as

$$R = -\frac{1}{2} \sum_{i=2}^{2n} (p_i - p_{i-1})(\zeta_i + \zeta_{i-1}), \tag{2}$$

where n points were used at each end. On the other hand, if one assumes that the pressure is essentially constant at p_0 and then drops suddenly to zero at the ends, then a first approximation to the wave resistance would be

$$R = p_0[\zeta(a) - \zeta(-a)]. \tag{3}$$

This formula (with $n = 1$) makes use of only one wave profile at each 'effective' end, namely at $x = \pm a$.

The calibration of the probe showed that the trace deflexion on the recorder was not precisely linear. This was undoubtedly due mainly to some basic non-linearity in the relation between the conductance of the probe and the depth of immersion, as well as to the way the probe was connected into the Wheatstone bridge. A linear approximation would have resulted in a maximum error of about 15% at the greatest deflexion encountered. Consequently the computer program was arranged to fit a parabola to the curve of trace deflexion *vs.* wave height. This matched the calibration curve with a measured worst error of 3·4% for all runs.

Twenty minutes settling time between runs was allowed. This was followed by a zero reading. The fan motor was then switched on and its speed adjusted to give the required cushion pressure, measured by means of tappings in the model base. A further 10 min were allowed for this change to settle, before initiating the run. The waiting period of 20 min was determined from the time required for the wave motion from the previous run to die out. The wave-height recordings were then found to be repeatable with the exception, naturally, of the

ripples which were caused by the turbulence in cushion air delivered by the fan. Of course, the theory does not account for this since it assumes a time-independent pressure acting on the water. One of the motivating factors behind the experiment was to see if this was an important feature.

A calibation was performed before, as well as after, a complete set of up to 18 runs (i.e. $n = 9$). The actual calibration curve used in the analysis of a particular run was obtained by a linear timewise interpolation between the two curves, which tended to differ by no more than 3% over a 9 h period. The response from the probe and electronics always tended in the same direction with increasing time and was more sensitive at the end of this period.

The tracks were surveyed by siting the probe at the two ends of the carriage and moving the carriage slowly over settled water. Thus the pitch angle ϵ of the carriage and model was found as a function of position along the track. The correction

$$\Delta R = \epsilon W, \tag{4}$$

W being the weight supported by the pressure, was then made by adding this to (2) and (3).

4. Theoretical analysis

Under the assumption of potential flow and linearized free-surface conditions, the theoretical wave resistance per unit width (Doctors & Sharma 1972) may be written as

$$R = \frac{1}{\pi\rho g}\int_0^t c(\tau)\,d\tau \int_0^\infty dw\, w^2[P^2+Q^2]\cos\left[(gw\tanh(wd))^{\frac{1}{2}}(t-\tau)\right]\cos\left[w\{s(t)-s(\tau)\}\right], \tag{5}$$

with

$$P+iQ = \int p(x)\exp(iwx)\,dx. \tag{6}$$

Here ρ is the water density, g is the acceleration due to gravity, d is the water depth, s is the distance travelled by the craft, and c is the instantaneous velocity at time t after the start of the motion.

The theory assumes that the pressure has been acting for all $t < 0$ and that the water is at rest at time $t = 0$, and thus corresponds to the experimental procedure of allowing the fan to run for some time before starting each run.

We may approximate the pressure distribution curve $p(x)$ by a series of straight lines. If, in addition, the distribution is symmetrical fore and aft, then (6) becomes

$$\left.\begin{aligned} P &= \frac{2}{w}\left[p_n\sin(wx_n)+\frac{1}{w}\sum_{i=1}^{n}\left(\frac{p_i-p_{i-1}}{x_i-x_{i-1}}\right)\{\cos(wx_i)-\cos(wx_{i-1})\}\right], \\ Q &= 0, \end{aligned}\right\} \tag{7}$$

where p_0 is measured at $x = x_0 = 0$.

We shall also test the idea of the equivalent pressure distribution suggested by the author previously, namely

$$p = \tfrac{1}{2}p_0[\tanh\{\alpha(x+a)\}-\tanh\{\alpha(x-a)\}], \tag{8}$$

where α is the pressure fall-off parameter and a is the effective half-length of the distribution, so that the weight supported by the pressure per unit width is given by

$$W = 2p_0 a. \tag{9}$$

In this case, it was shown that (6) gives

$$P = p_0 \pi \sin(aw)/\alpha \sinh(\pi w/2\alpha). \tag{10}$$

In order to make (8) equivalent to the actual pressure distribution, values of p_0, a and α must be found. We take the nominal pressure p_0 to be the essentially constant value over the central region of the cushion. The nominal half-length is given by a and is found by balancing the weight via (9). This leaves one degree of freedom, namely the choice of the amount of 'spread' of the cushion beyond the nominal length. The value ΔW of this lift supported beyond $x = \pm a$ may be related to the pressure fall-off parameter α in the following way:

$$\begin{aligned}\Delta W &= 2\int_a^\infty p(x)\,dx \\ &= p_0 \int_a^\infty [\tanh\{\alpha(x+a)\} - \tanh\{\alpha(x-a)\}]\,dx \\ &= p_0[2\alpha a - \ln\cosh(2\alpha a)]/\alpha \\ &\doteq p_0(\ln 2)/\alpha \quad \text{for} \quad \alpha a > 2.\end{aligned}$$

Thus

$$\alpha a = 0{\cdot}3466\, W/\Delta W. \tag{11}$$

5. Results

The pressure distribution generated on a groundboard by the model is shown in figure 3. The pressure was measured by means of static tappings in a horizontal board set at three different heights relative to the model base. This situation is a simplification of that existing under the craft while under way. Ideally one should construct a number of groundboards with the same wavy shapes as the water surface at various instants of time. The pressure distribution on these boards could then be fed into a modified theory allowing for a pressure varying with time. Even this procedure would assume that the cushion-pressure distribution varies quasi-steadily with time, and it neglects spray generation. The complication of using a non-horizontal groundboard may be gauged by referring to the pressure distributions measured by Hogben (1966) on a tilted groundboard under a circular-platform model. The pressure is seen to be essentially constant for $x < 3$ in. but the details of the fall-off at the edge depend on the height h of the model above the ground. For the intermediate and largest height there is an initial rise in pressure, that is $p/p_0 > 1$, owing to the interaction of the air jet with the ground. The effective length [given by (9)] is seen to increase slightly with height. In addition, the sharpness of the distribution, given by (11), increases. Also shown is (8) for the case $h = 1{\cdot}41$ in., the clearance for all the experiments.

A typical set of wave profiles is displayed in figure 4. The effective length a

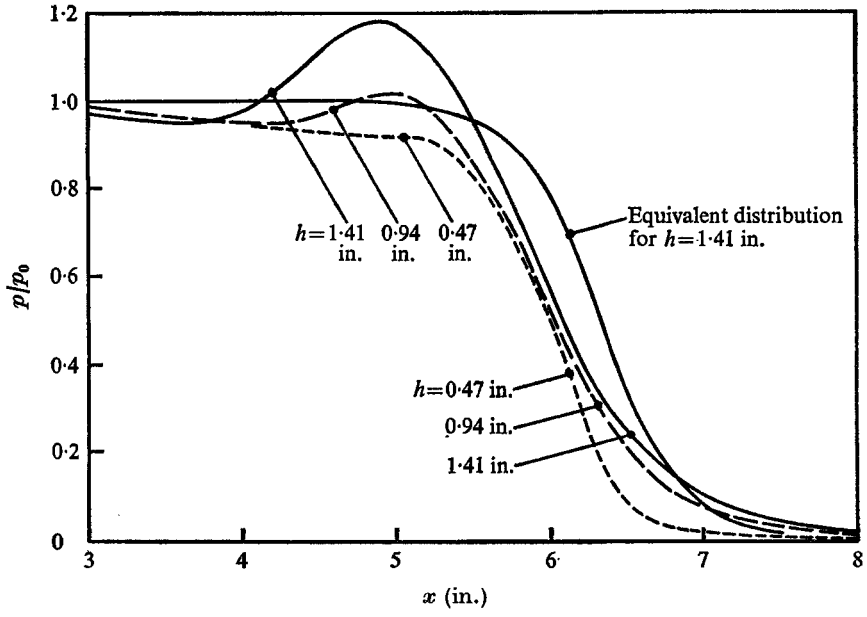

FIGURE 3. Measured cushion-pressure distributions on groundboard.

h (in.)	0·47	0·94	1·41
a (in.)	5·83	6·09	6·34
αa	7·15	8·10	11·88

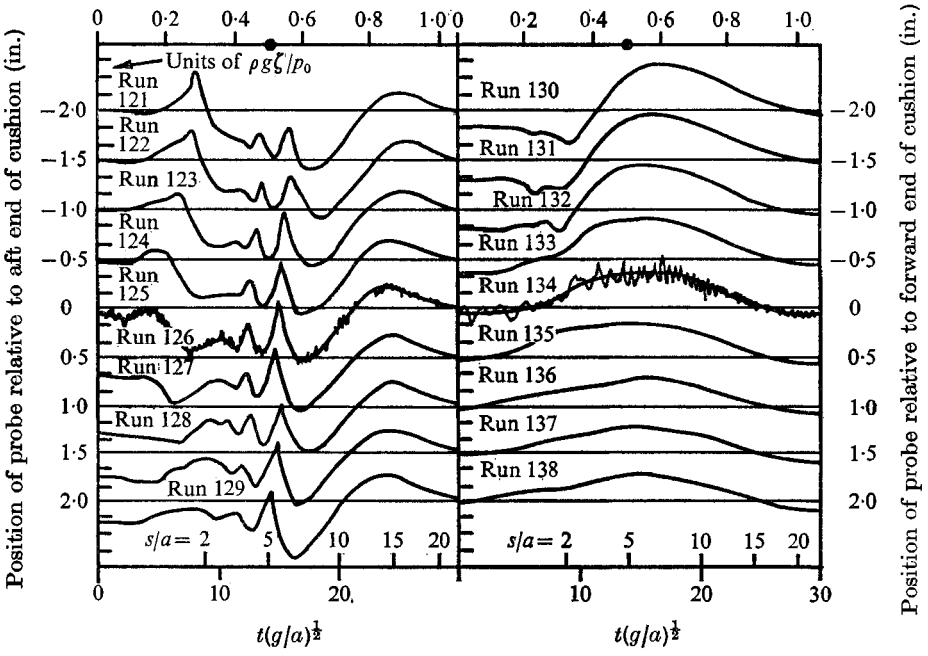

FIGURE 4. Set of experimental wave profiles. d/a = 0·5, $\dot{c}/g$ = 0·05, $p_0/\rho ga$ = 0·02, h = 1·41 in. (The points on the Froude-number scale indicate the positions of the steady-state humps.)

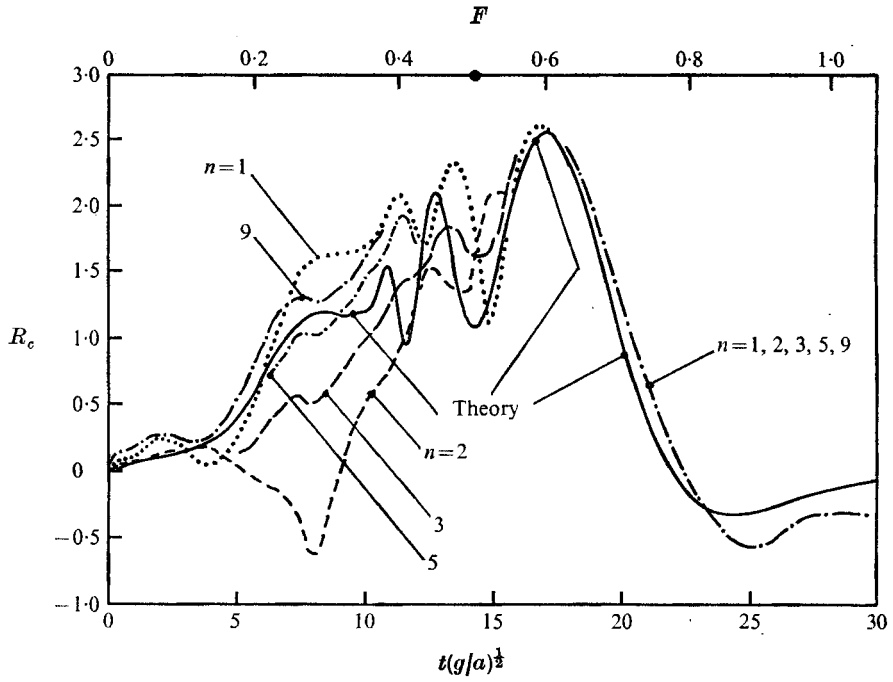

FIGURE 5. Effect of number of wave profiles used in wave-resistance integration. Conditions as in figure 4. (The point on the Froude-number scale indicates the steady-state hump.)

was used to non-dimensionalize the time t and distance s. In the region near the forward end of the craft (runs 130–138) there is generally a positive wave generated, which then dies out at a sufficiently high speed. The depression of the water at $t = 0$ should, of course, correspond to the pressure in figure 3. This is not always precisely the case, as, for example, in run 127, where it is too large. This is presumably due to unsteadiness of the water surface. (The curves have been smoothed in figure 4; the original records, which show the ripples generated by the fan air, are shown for runs 125 and 134 only.) Furthermore, the pressure distribution over water will be different from that over the groundboard, owing to the water surface's deflexion.

Wave profiles near the aft end (runs 121–129) illustrate the more complicated waves generated there. There is a general shift of the hump to an earlier time for profiles further ahead, as one might expect.

Figure 5 displays the wave-resistance coefficient, defined by

$$R_c = \frac{R}{W}\frac{\rho g a}{p_0}, \tag{12}$$

as a function of time. The experimental curves were obtained by analysis of differing numbers of the profiles in figure 4. Thus $n = 1$ corresponds to the use of runs 125 and 134 (i.e. values at the effective ends of the cushion) only, by means of (3). The case of $n = 2$ used runs 121, 129, 130 and 138. That of $n = 3$ used those for $n = 2$ as well as the two for $n = 1$, and so on. Comparison is also made with the theory. The experimental wave profiles for an acceleration of

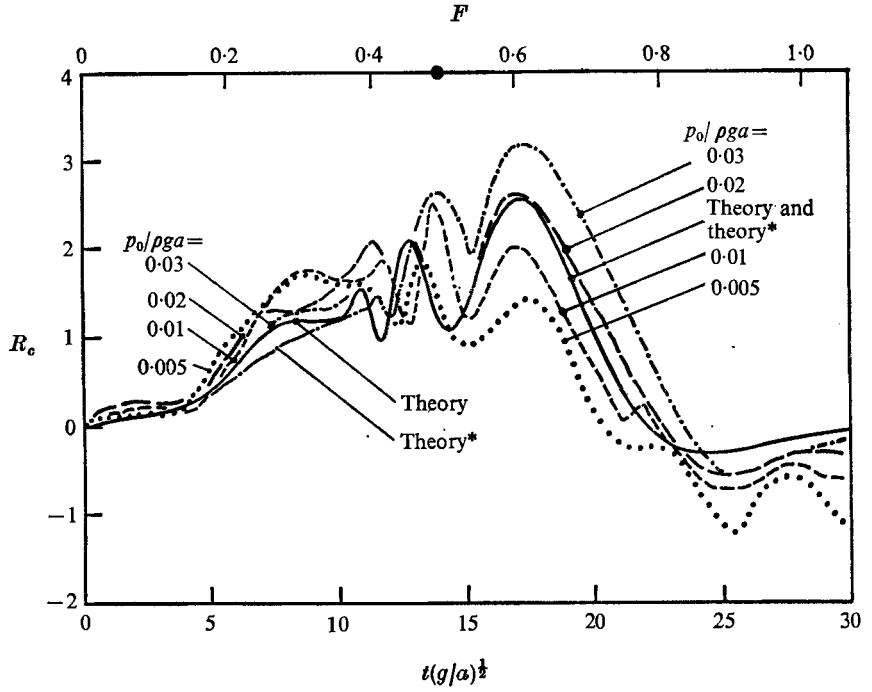

FIGURE 6. Test of linearity of the theory. $d/a = 0{\cdot}5$, $\dot{c}/g = 0{\cdot}05$, $n = 9$, $h = 1{\cdot}41$ in. An asterisk indicates the theory using the equivalent pressure distribution with $\alpha a = 11{\cdot}88$. (The point on the Froude-number scale indicates the position of the steady-state hump.)

$\dot{c}/g = 0{\cdot}05$ (shown here and later) and those for $\dot{c}/g = 0{\cdot}1$ and $0{\cdot}15$ (in later figures) were digitized with 78, 52 and 69 points, respectively. In all cases the theoretical wave resistance, given by (5), was computed using 257 points in the time integral. The wavenumber integral was truncated at $wa = 40$, and was performed using 382, 319 and 215 points for the three levels of acceleration respectively. The pressure distribution in (7) was represented by 22 points. (These computing parameters give an estimated error of less than 0·001 in R_c.)

The experimental curves are all very close to one another in the main-hump region and above it, corresponding to $t(g/a)^{\frac{1}{2}} > 16$. The theory in this region compares well and the predicted negative wave resistance referred to in the introduction is also verified. At the lower speeds, the differences are greater owing partly to shifting in the phasing of the oscillations. Surprisingly, the curve for $n = 1$ is somewhat better than those for $n = 2$ or 3 in this region.

The linearity of the theory is illustrated in figure 6, where different pressure levels are tested. To a certain extent the forms of these curves are similar, particularly in the hump region. However, the peak resistance, for example, increases faster than the square of the pressure predicted by the linear theory. In fact, at the hump, $R_c \propto p_0^{0{\cdot}44}$ approximately, so that $R \propto p_0^{2{\cdot}44}$. However, it must be pointed out that the experimental analysis used the pressure distribution measured at rest over the groundboard. This will be increasingly distorted as the pressure is raised.

The theory using the equivalent pressure distribution (8) is also shown, and

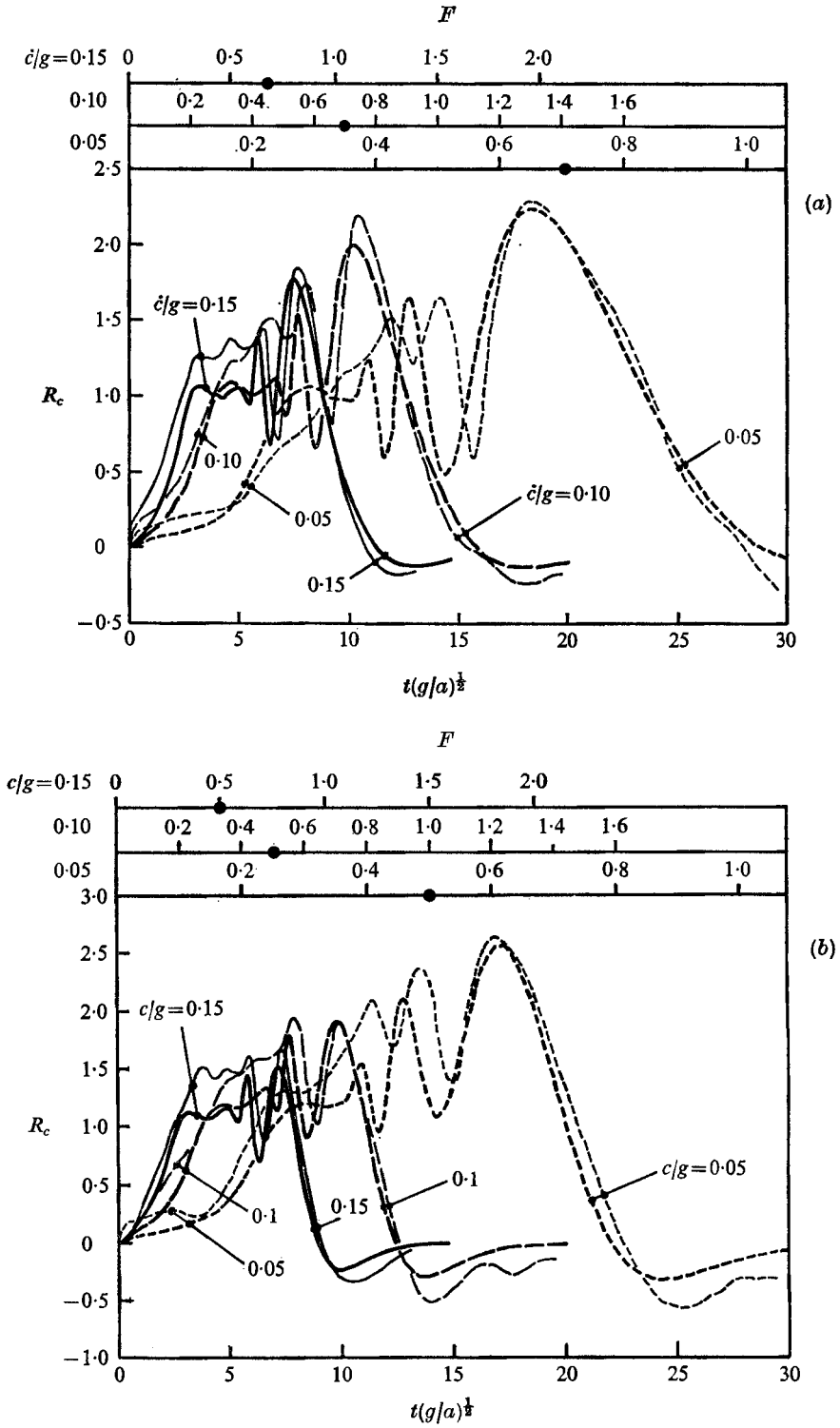

FIGURES 7 (*a*, *b*). For legend see facing page.

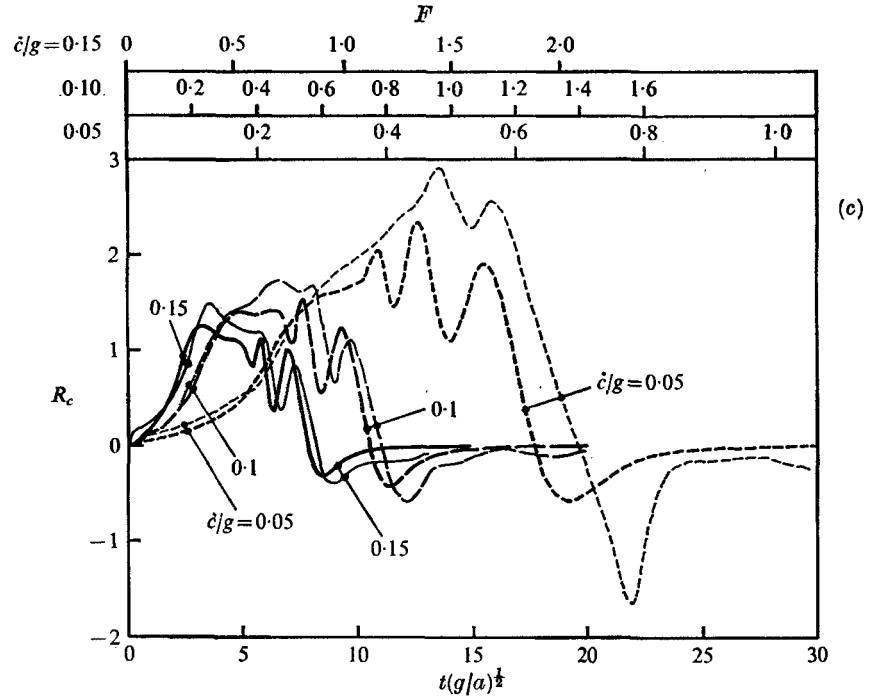

FIGURE 7. Comparison of experiment (thin curves) with theory (thick curves). $p_0/\rho ga = 0{\cdot}02$, $h = 1{\cdot}41$ in., $n = 5$ (except for $\dot{c}/g = 0{\cdot}05$ in (*b*), for which $n = 9$). (*a*) $d/a = 1{\cdot}0$. (*b*) $d/a = 0{\cdot}5$. (*c*) $d/a = 0{\cdot}25$. (The points on the Froude-number scales indicate the positions of the steady-state humps.)

is seen to differ little from the theory using the actual distribution, except in part of the low-speed range.

Finally, figures 7(*a*), (*b*) and (*c*) compare the theory for the resistance with experiments for three depths, respectively. Each figure depicts results for three levels of acceleration. The agreement is generally a little better for the higher accelerations, with regard to the phase of the oscillations. Furthermore the agreement improves as the depth is increased. This is not surprising, since the large wave amplitudes will have more time to grow and the resulting nonlinearities are expected to be accentuated as the steady state is approached. It is gratifying, further, to note that the correct number of humps and hollows is essentially predicted for all cases in figure 7. This is in contrast to steady-state experiments cited earlier.

6. Concluding remarks

The experiments are generally encouraging, mainly with regard to the confirmation of the general form of the theoretical curves of wave resistance. The principal feature of the theory which is not precisely confirmed by the experiments is that of linearity; the wave resistance in the region of the main hump and hollow increases somewhat faster than the predicted square of the nominal cushion pressure.

The nonlinearity depicted in figure 6 is, in fact, worse than was anticipated, and may be due to the method of analysis. The pressure, being taken as that over the groundboard, is only correct for low values, and hence implies an *a priori* assumption of linearity [although (1) makes no such assumption]. The problem of water deflexion *at rest* was discussed by Hogben (1967). It might be pointed out that all current techniques for analysing wave patterns, described, for example, by Eggers *et al.*, also implicitly assume linearity, as well as vanishing viscosity. It had been thought that the results in figure 6 would be improved as $p_0/\rho ga \to 0$, but presumably other effects must be playing an important role.

For example, at the main hump, when $t(g/a)^{\frac{1}{2}} = 17$, for $p_0/\rho ga = 0{\cdot}005$ (see figure 6) the stagnation pressure of the incident air is 0·086 of the cushion pressure. If one assumes that this effect would depress the water surface in the bow region of the model, on hydrostatic considerations alone, then it would amount to a reduction in R_c of 0·043. However, this could only be a partial explanation of the 1·14 discrepancy in R_c at this value of the pressure.

A second factor which might be important at low cushion pressures is surface tension, which would alter the probe readings.

The general rise in the measured hump resistance coefficient with pressure could be explained by cross-flow within the cushion.† The mean longitudinal water slope is theoretically proportional to p_0. As a result of this water-surface distortion, there will be a general flow of air aft from the forward nozzle. Thus there will be, in essence, a two-dimensional expansion duct, the expansion ratio of which is proportional to p_0. The resulting Bernoulli effect will increase the pressure at the stern relative to that at the bow and cause an increase in the measured wave resistance. If one took this *modification* to the original pressure to be proportional to p_0, and to be of second order, then the wave-resistance coefficient at, say, the hump speed would be given by

$$R_c = A + Bp_0.$$

This linear trend is seen to be not unrealistic in figure 6. (It is pointed out that the power-law variation of R_c with respect to p_0 previously referred to is simply a curve fit and has no particular physical significance.)

Another point to be considered is the disturbance caused by the probe, which alters its electrical output. If this is the same for points fore and aft of the model, then it can be shown that this effect precisely cancels out in (2). However, the probe disturbance will not be entirely the same, since its velocity through the water depends on the water motion as well as the carriage motion. Possibly the effect is dependent on the value of $p_0/\rho ga$ when viscosity and surface tension are also considered. Incidentally, some thought was given to using a stationary wave-height probe. Apart from the additional complication of the analysis of the recordings associated with it, the stationary probe would be at least as prone to surface-tension distortion effects at low pressures.

Regarding future work, the next stage is to test a three-dimensional model. It is suggested that the agreement with theory will be better since the wave interference effects will be reduced in this case. If the current method of wave

† The author is grateful to one of the referees of the paper for suggesting this discussion.

analysis is used, then wave profiles will have to be taken at different transverse positions, as well as longitudinal ones, greatly increasing the experimental effort.

The writer wishes to express his deep gratitude to Mr R. B. Frost of the Hydraulics Laboratory for considerable assistance with the design of the equipment. He is also grateful to Mr B. C. Motson of the Aerodynamics Laboratory for his help, and would like to acknowledge the financial support of the Australian Research Grants Committee.

REFERENCES

BARRATT, M. J. 1965 The wave drag of a hovercraft. *J. Fluid Mech.* **22**, 39–47.

DOCTORS, L. J. 1972 The forces on an air-cushion vehicle executing an unsteady motion. In *Proc. 9th Symp. on Naval Hydrodyn., Paris*, pp. 35–97. Washington: Office of Naval Research.

DOCTORS, L. J. & SHARMA, S. D. 1972 The wave resistance of an air-cushion vehicle in steady and accelerated motion. *J. Ship. Res.* **16**, 248–260.

DOCTORS, L. J. & SHARMA, S. D. 1973 The acceleration of an air-cushion vehicle under the action of a propulsor. *J. Ship Res.* **17**, 121–128.

EGGERS, K. W. H., SHARMA, S. D. & WARD, L. W. 1967 An assessment of some experimental methods for determining the wavemaking characteristics of a ship form. *Trans. Soc. Naval Archit. & Mar. Engrs*, **75**, 112–157.

EVEREST, J. T. 1966*a* The calm water performance of a rectangular hovercraft. *Nat. Phys. Lab.* (*Ship Div.*) *Rep.* no. 72.

EVEREST, J. T. 1966*b* Shallow water wave drag of a rectangular hovercraft. *Nat. Phys. Lab.* (*Ship Div.*) *Rep.* no. 79.

EVEREST, J. T. & HOGBEN, N. 1966 Measurements of the wave pattern resistance of a rectangular hovercraft. *Nat. Phys. Lab.* (*Ship Div.*) *Tech. Memo* no. 147.

EVEREST, J. T. & HOGBEN, N. 1967 Research on hovercraft over calm water. *Trans. Roy. Inst. Naval Archit.* **109**, 311–326.

EVEREST, J. T. & HOGBEN, N. 1969 A theoretical and experimental study of the wavemaking of hovercraft of arbitrary planform and angle of yaw. *Trans. Roy. Inst. Naval Archit.* **111**, 343–365.

EVEREST, J. T. & WILLIS, R. C. 1968 Experiments on the skirted hovercraft running at angles of yaw with special attention to wave drag. *Nat. Phys. Lab.* (*Ship Div.*) *Rep.* no. 119.

HAVELOCK, T. H. 1932 The theory of wave resistance. *Proc. Roy. Soc.* A **138**, 339–348.

HOGBEN, N. 1965 Wave resistance of steep two-dimensional waves. *Nat. Phys. Lab.* (*Ship Div.*) *Rep.* no. 55.

HOGBEN, N. 1966 An investigation of hovercraft wavemaking. *J. Roy. Aero. Soc.* **70**, 321–329.

HOGBEN, N. 1967 Hovering craft over water. In *Advances in Hydroscience*, vol. 4, pp. 1–72. Academic.

LUNDE, J. K. 1951 On the linearized theory of wave resistance for a pressure distribution moving at constant speed of advance on the surface of deep or shallow water. *Skipsmodelltanken, Norges Tekniske Høgskole, Trondheim, Rep.* no. 8 (in English).

NEWMAN, J. N. & POOLE, F. A. P. 1962 The wave resistance of a moving pressure distribution in a canal. *Schiffstech.* **9**, pp. 21–26 (in English).